Comparison study on a large-scale free-piston Stirling cryocooler

Hangyu Ma[1,2], Guoyao Yu[1,3*], Haojie Sun[1], Ying Ma[1], Wei Dai[1,2] and Ercang Luo[1,2]

[1] CAS Key Laboratory of Cryogenics, Technical Institute of Physics and Chemistry, Beijing 100190, China
[2] University of Chinese Academy of Sciences, Beijing 100049, China
[3] Institute of Optical Physics and Engineering Technology, Qilu Zhongke, Jinan 251000, China

[*]E-mail: gyyu@mail.ipc.ac.cn

Abstract. Large-scale free-piston Stirling cryocoolers, capable of delivering several hundred watts of cooling power at 80 K, have significant potential applications in boil-off gas re-liquefaction and precooling processes. Recently, we proposed a novel parallel regenerator layout aimed at suppressing local acoustic streaming, which could enable further scaling of the cryocooler while maintaining high thermal efficiency. Numerical modeling was performed, and an experimental prototype was developed based on this design. Experimental results demonstrated reasonable agreement with the numerical predictions in terms of cooling power. However, discrepancies in thermal efficiency were observed, likely due to inconsistencies among the individual regenerators.

1. Introduction

A cryocooler-equipped container provides a closed-loop, on-demand cooling solution, eliminating the need for periodic cryogen replenishment. These cryocoolers, designed to deliver cooling capacities ranging from hundreds to thousands of watts at liquid nitrogen temperatures, are increasingly critical for applications in biomedical engineering, semiconductor manufacturing, superconductivity, and battery fire suppression. They offer efficient, compact solutions for maintaining cryogenic temperatures in systems where size, performance, and rapid cooling are paramount. Among available technologies, Stirling-cycle cryocoolers are particularly effective due to their compact design and versatile interfaces [1]. Currently, rotary Stirling cryocoolers, pulse tube cryocoolers, and free-piston Stirling cryocoolers represent the primary viable options. As illustrated in Figure 1, both rotary Stirling and pulse tube cryocoolers demonstrate high efficiency and reliability for cooling capacities around or below 10 W at 77 K, attributed to their simpler structures [2]. However, for cooling requirements between 100 W and 1000 W, free-piston Stirling cryocoolers exhibit superior overall performance. Theoretical calculations suggest potential for further performance enhancements, yet comprehensive investigations in this area remain limited.

In our previous study, numerical and experimental optimization of mean pressure and operating frequency was conducted on a large-scale free-piston Stirling cryocooler, achieving a maximum cooling power of 350 W at 80 K with a relative Carnot efficiency of 26.8% based on input electrical power [3]. Subsequent optimization of the displacer parameters yielded improved performance, with experimental results demonstrating a cooling power of 406 W at 80 K and a

relative Carnot efficiency of 27.8%, as shown in Figure 2. Although these efforts reduced the discrepancy between experimental and numerical results, a non-uniform circumferential temperature distribution in the regenerator's midsection, illustrated in Figure 3, remains a significant barrier to further performance enhancements. This study represents the first attempt to address this issue by proposing a novel parallel-regenerator configuration. The design methodology is detailed in Section 2, followed by initial experimental results and discussion. Conclusions are presented in the final section.

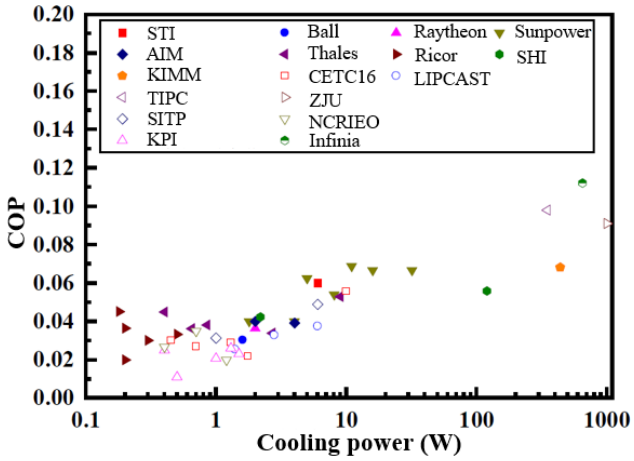

Figure 1. Published results of cryocooler COP Vs. cooling power at liquid nitrogen temperature.

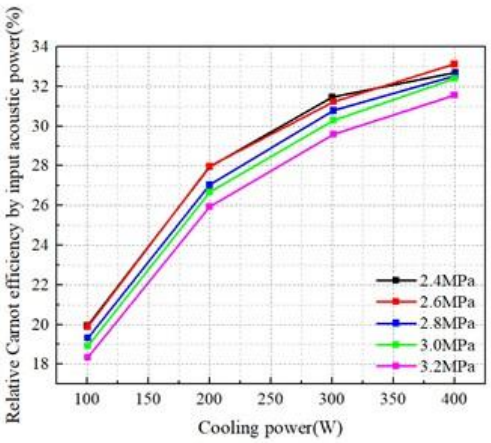

Figure 2. Dependence of relative Carnot efficiency on cooling power under different mean pressure.

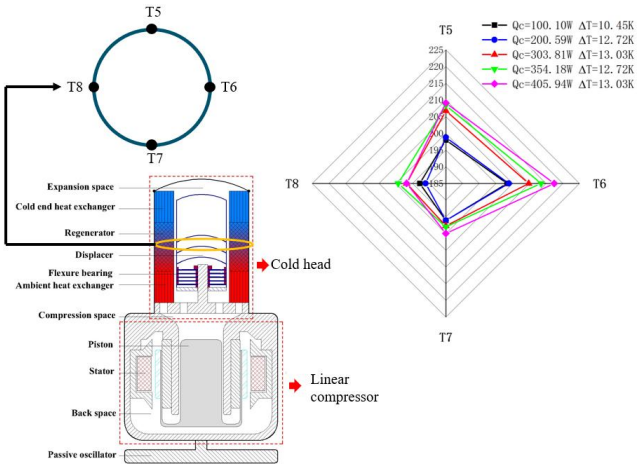

Figure 3. Temperature distribution in the middle of the regenerator under different cooling power.

2. Method and design

2.1 Design method

As illustrated in Figure 3, the free-piston Stirling cryocooler (FPSC) investigated in this study comprises a linear compressor and a cold head, with dimensions detailed in Table 1. The cold head adopts a coaxial layout to minimize its footprint and accommodate various loads. Within this

configuration, a cold-end heat exchanger (CHX), regenerator (REGEN), and ambient heat exchanger (AHX) are arranged in series within the annular space surrounding the displacer (DISP). This coaxial arrangement generally mitigates non-uniform radial temperature and flow distributions in the regenerator compared to an in-line configuration. However, for cooling capacities exceeding 100 W at 80 K, the regenerator's compact, stubby geometry exacerbates local acoustic streaming, as previously discussed in Ref. [4].

If we pay one deeper look at the key parameters of the FPSC, i.e., the regenerator aspect ratio, which is defined to be:

$$\alpha = \frac{L}{D} \tag{1}$$

L and D denote the length and diameter of the regenerator, respectively. Herein for annual structure, D stands for hydraulic diameter. The product for the current design is only 0.64, well below that of a small-scale one (typically around 5~10). Ref. [4] employed a combined approach of second-order thermoacoustic analysis and linear perturbation to elucidate the destabilizing mechanisms within the regenerator. While our experimental observations of the midplane temperature distribution align closely with their assumptions, calculating the instability threshold remains challenging due to limited measurement data, particularly for acoustic streaming and associated heat flux.

Table 1. Dimensions of the current FPSC.

Component	Specifications	Component	Specifications
Expansion space	45 cc	Compression space	300 cc
CHX	Radial-fin type Length: 30 mm Fin gap :0.3 mm Fin radial height: 19 mm	AHX	Radial-fin type Length: 35 mm Fin gap :0.5 mm Fin radial height: 16.25 mm
Regenerator	Length: 60 mm i.d.: 84 mm o.d.: 124 mm Screen mesh: 300# Mesh wire diameter: 31 μm Porosity: 0.76	Displacer	Rod diameter: 25 mm Moving mass: 0.97 kg Spring stiffness: 113.3 kN/m

Inspired by the mechanism of local acoustic streaming driven by transverse mean-temperature perturbations, a regenerator array comprising multiple identical small-diameter regenerators arranged in parallel is proposed as a promising approach to enhance transverse thermal and hydrodynamic communication within the regenerator. Figure 4 provides a schematic of this novel design. Unlike the conventional coaxial-pipe configuration [5], this parallel-

regenerator design accommodates various regenerator packing materials and may mitigate shuttle losses to some extent.

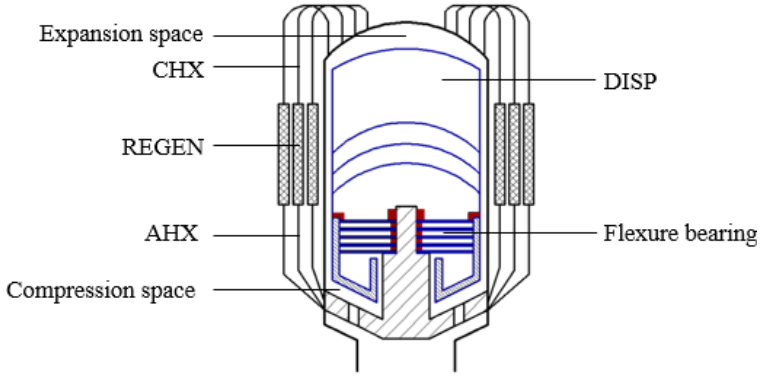

Figure 4. Schematic drawing of the parallel-regenerator design.

2.2 Design details

In order to determine the number of regenerators, simulations were implemented by using SAGE [6] and thermoacoustic analysis, with the modeling interface depicted in Figure 5. As a preliminary attempt, a simplified approach based on equal division of the annular regenerator's cross-sectional area was employed, as detailed in Table 1, given by:

$$S_{\sin gle} = \frac{S_{annual}}{n} \tag{2}$$

where S_{single}, S_{annual} and n represent cross-sectional area of the single regenerator of the regenerator array, cross-sectional area of the original annular regenerator, and number of the regenerators, respectively. From the perspective of thermoacoustics, the fundamental acoustic characteristics remains almost the same for tubes owning equivalent cross-sectional area.

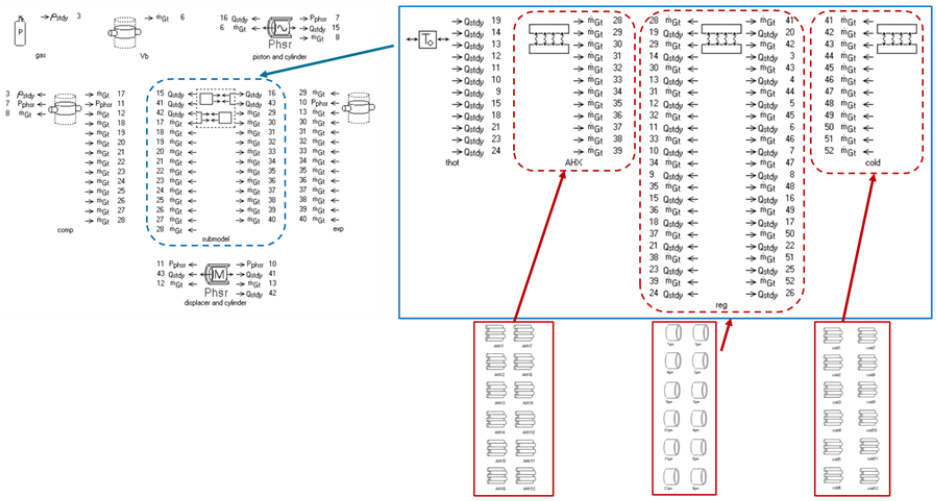

Figure 5. Snapshot of the modelling interface.

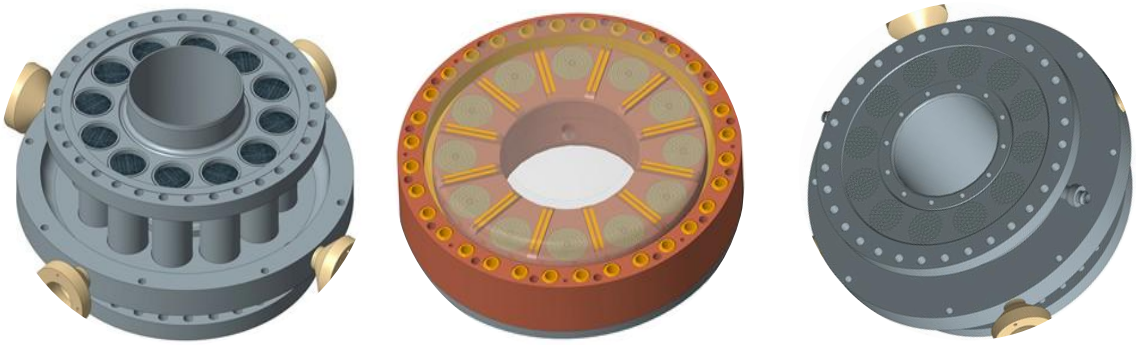

(a) regenerator assembly **(b) CHX assembly** **(c) AHX assembly**

Figure 6. Snapshot of the novel design.

Table 2. Dimensions of the regenerator and heat exchangers.

Component	Specifications
CHX	Copper tube-bundle type Length: 35 mm Tube inner diameter : 1.0 mm Tube wall thickness: 0.5 mm Number of tubes: 100 (total 1200)
AHX	Stainless-steel tube-bundle type Length: 30 mm Tube inner diameter : 1.0 mm Tube wall thickness: 0.3 mm Number of tubes: 61 (total 732)
Regenerator	Length: 60 mm Tube inner diameter: 26 mm Tube wall thickness: 1.5 mm Number of tubes: 12 Screen mesh: 300# Mesh wire diameter: 31 μm Porosity: 0.76

Prior to finalizing the number of regenerators, additional factors warrant consideration, including flow straightening between regenerators and adjacent heat exchangers, as well as ensuring sufficient gas-solid contact area in the heat exchangers. Typically, radial-fin copper heat exchangers are preferred for both the cold-end heat exchanger and ambient heat exchanger due to their high thermal conductivity and capacity, which enhance resistance to thermal fluctuations. However, directly integrating radial-fin heat exchangers into the proposed parallel-regenerator design poses challenges in flow redistribution as gas shuttles between the regenerator and heat exchangers. While increasing the number of regenerators could alleviate this issue, it introduces complications such as inconsistencies within individual regenerators and excessive heat

conduction through regenerator walls. To address these challenges, a tube-bundle configuration is proposed, utilizing copper for the CHX and stainless steel for the AHX, striking a balance between jet-flow suppression and adequate gas-solid contact area. Furthermore, each regenerator is paired with dedicated CHX and AHX units, forming an independent thermoacoustic core. This design is illustrated in Figure 6.

A configuration of 12 regenerators was selected to further balance manufacturing and assembly convenience, with detailed dimensions provided in Table 2. A comparative analysis of fundamental performance between the parallel-regenerator and conventional annular-regenerator designs was conducted. The results suggest that, for an equivalent inlet pressure ratio, the parallel-regenerator design achieves higher cooling power due to reduced void volume, while maintaining comparable relative Carnot efficiency, defined as follows:

$$\eta_{RelativeCarnot} = \frac{Q_C(\frac{T_A}{T_C}-1)}{W_a} \tag{3}$$

where Q_C and W_a are the cooling capacity and net input acoustic power, respectively. T_A and T_C represent the solid temperature of the AHX and CHX, respectively.

3. Experiments and discussion

To validate the proposed design, a parallel-regenerator free-piston Stirling cryocooler was constructed and tested. Figure 7 presents photographs of the cryocooler and its cold head. The system was charged with an initial helium pressure of approximately 3.0 MPa. Multiple PT100 thermometers and electric cartridge heaters were installed on the CHX to monitor and control temperature. Pressure sensors were placed in the compression space to measure both mean pressure and pressure oscillations. Additionally, an accelerometer was mounted on the displacer to measure displacement, enabling indirect calculation of local acoustic power.

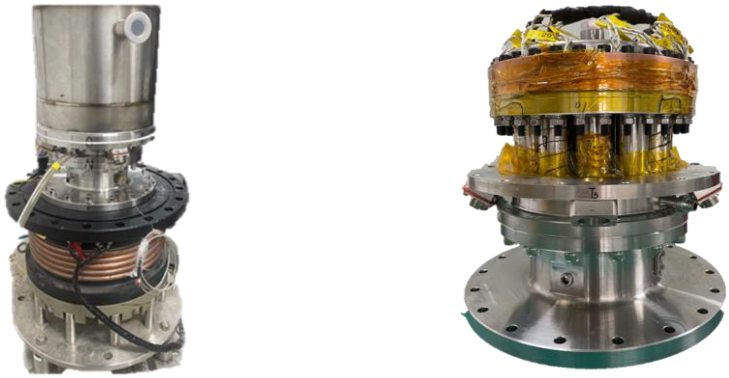

(a) FPSC **(b) cold head**

Figure 7. Photographs of FPSC and cold head.

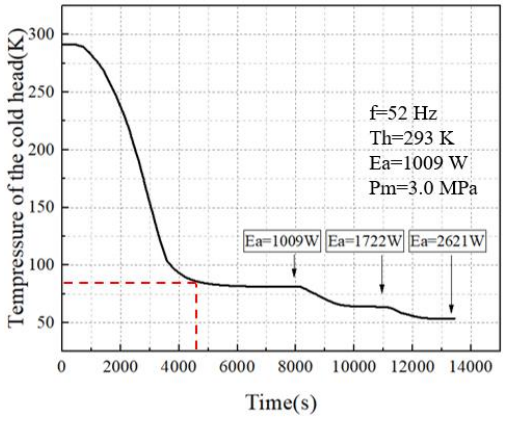

Figure 8. Typical Cool-down curve.

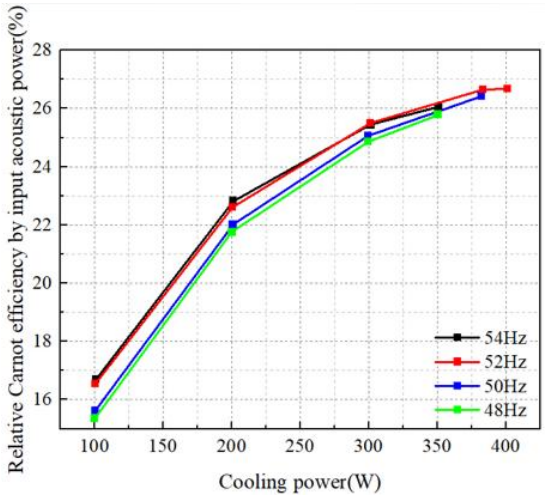

Figure 9. Dependence of relative Carnot efficiency on cooling power under different frequency.

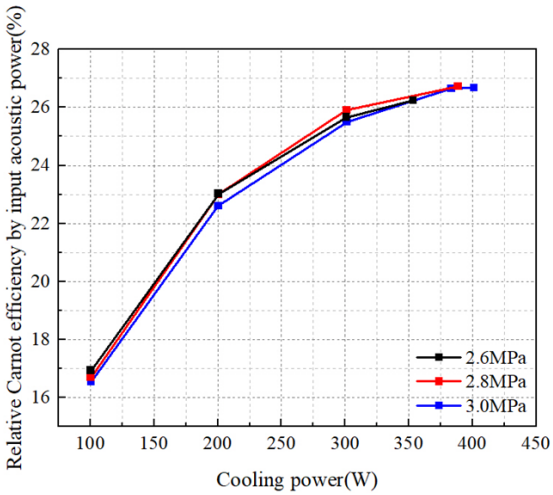

Figure 10. Dependence of relative Carnot efficiency on cooling power under different charge pressure.

The cool-down process was initially evaluated from ambient temperature without an applied heat load. Figure 8 illustrates a typical cool-down curve. With an initial input acoustic power of 1009 W supplied to the cold head, the system achieved a temperature of 80.7 K in approximately one hour. The lowest temperature, 52.8 K, was reached when the input acoustic power was increased to 2621 W.

Refrigeration performance was evaluated under varying operating frequencies and charge pressures. Figure 9 illustrates the effect of operating frequency on the relative Carnot efficiency at 80 K as a function of cooling power, with a charge pressure of 3.0 MPa. As cooling power increases, the acoustic power-based relative Carnot efficiency rises correspondingly but exhibits clear saturation as the cooling power approaches 400 W. The operating frequency appears to have minimal impact on this trend, particularly at peak cooling power. Consistent with previous experimental results for the annular-regenerator FPSC shown in Figure 2, the performance curve demonstrates low sensitivity to charge pressure variations, as depicted in Figure 10. This behavior is attributed to the minor variation in acoustic impedance when the charge pressure ranges from 2.6 MPa to 3.0 MPa. At higher charge pressures, however, the shift in acoustic

impedance and associated clearance-seal losses (also indicated in Figure 2) degraded the performance, and thus experiments were not conducted. Across these experiments, a maximum cooling power of 400 W was achieved at a charge pressure of 2.8 MPa and an operating frequency of 52 Hz, corresponding to a peak acoustic power-based relative Carnot efficiency of 27%.

4. Conclusion

A parallel-regenerator configuration was proposed for a large-scale free-piston Stirling cryocooler to enhance performance when scaling up to a cooling power of 1000 W at liquid nitrogen temperature. In this design, each regenerator is paired with dedicated heat exchangers, and a configuration of 12 thermoacoustic cores was adopted as a compromise to balance performance and practicality. Experimental results indicate that the cooling power achieved is comparable to that of the previous annular-regenerator design. However, the relative Carnot efficiency exhibited significant degradation, primarily attributed to inconsistencies among the regenerators and elevated thermal resistance in the heat exchangers.

Acknowledgments

This work was financially supported by the National Natural Science Foundation of China under Contract No. 51876214 and 52306031. The authors are also grateful to the financial and technical support from Lihan cryogenics and Zhongke thermoacoustics.

References

[1] R. Radebaugh 2019 *J Phys: Condens Matter*, **21(16)** 164219
[2] Yun Qi 2024 Doctoral thesis, Zhejiang University
[3] Shunmin Zhu, Guoyao Yu, Xiaowei Li, Wei Dai and Ercang Luo 2020 *Applied Thermal Engineering* **174** 115101
[4] J H So, G W Swift and S Backhaus 2006 *J Acoust Soc Am* **120** 1898-1909
[5] S Masuyama, K Matsumoto and T Numazawa 2021 *J Phys: Conference Series* **1857** 012007
[6] Gedeon D 2014 10th ed. Athens, OH: Gedeon Associates